Shock Compression and the Melting Curve for Argon*

Marvin Ross
Lawrence Livermore Laboratory, University of California, Livermore, California 94550
(Received 5 March 1973)

Recent experimental shock-compression work on solid argon is analyzed to obtain an intermolecular potential. The intermolecular potential is used to compute the high-pressure melting curve. The author predicts that the shock-compression curve crosses the melting line at 50 kbar and just under 700 °K, but that the inherent experimental error is too large for the transition to be seen as a break in the PV or $U_s U_p$ curves.

I. INTRODUCTION

During the past 20 years, explosive shock-wave experiments on liquids and solids have yielded a large body of equation-of-state information for densities and pressures that could not be attained by static methods. Because of the fundamental nature of condensed rare gases, their equations of state have been studied extensively in this laboratory and at Los Alamos.[1-5] In previous papers the results of these experiments have been interpreted in order to determine intermolecular forces and to study the effect of electronic excitation on the observed properties.[4] In principle, it should also be possible to use shock-wave methods to determine melting curves.

In a shock-compression experiment, measurements are made of the shock velocity U_s and the particle velocity U_p. The pressure and volume are related to U_s and U_p by the Rankine-Hugoniot relations

$$P = U_s U_p / V_0, \quad V = V_0(1 - U_p/U_s),$$

where V_0 is the initial volume.

Recently, Dick, Warnes, and Skalyo[5] carried out an experiment in which they shock-compressed solid argon from an initial state of 1 bar and 75 °K up to 645 kbars and a density greater than twice that of the initial solid. Because a shock experiment is highly irreversible, the compression is accompanied by a large temperature rise. In the case of solid argon for example, the final temperature at 645 kbars is 21 500 °K and the material is fluid. At some pressure the shock-compression curve (Hugoniot) will cross the melting curve, and in principle this phase transition should be detectable as a discontinuity in the $U_s U_p$ curve. The shock wave has different characteristic velocities in each phase. Since most $U_s U_p$ curves are linear, changes in them are readily observed.

In the experiments of Dick *et al.*, the $U_s U_p$ curve obtained could not be represented by a single curve; it had to be fit by two linear curves that intersected near 250 kbars. Their results are shown by the circles in Fig. 1. The dashed line is an extension of the low end of the experimental curve and is included to illustrate the nonlinearity. These authors then suggested on the basis of the $U_s U_p$ data that they had crossed the melting curve at 250 kbars.

In the present paper we wish to suggest an alternate interpretation and present what we believe is the correct relationship between the argon melting curve and Hugoniot.

To calculate Hugoniots and melting curves we need models of the solid and liquid, and also an intermolecular potential. The statistical models of the two phases are discussed in Sec. II. These models are then used in Sec. III to find an intermolecular potential that will reproduce the shock-wave experiments. We shall assume that the intermolecular potential is additive by pairs, but since this may not be exactly correct we shall understand that our pair potential is actually an effective one. Now, having models of the liquid and solid, and an effective intermolecular potential for compressed argon, we can go on to calculate its melting curve—which is done in Sec. IV. In Sec. V we use the theoretical approximation of Hafmeister to calculate the intermolecular potential between argon atoms.

II. STATISTICAL MODELS OF SOLID AND LIQUID

The models of the solid and liquid are, respectively, the Lennard-Jones–Devonshire (LJD) model[6] and the Mansoori-Canfield[7] (MC) perturbation theory of the fluid. The LJD model was first proposed as a model of the liquid, but it has more recently been understood to be an excellent model of the solid. In this model an atom is confined to a cell and moves about in the spherically averaged field of its stationary neighbors. The model is fully discussed by Barker,[8] and its validity as an excellent solid model is based on comparisons with Monte Carlo results for solids. In the Mansoori-Canfield perturbation theory of the fluid, a system of hard spheres is used as a reference, and the

perturbation consists of the atoms interacting under the influence of an intermolecular potential and a hard-sphere radial distribution function. In the lowest order of the theory, we can write the Helmholtz free energy of the fluid as

$$\frac{F}{kT} = \frac{F^0(d, V)}{kT} + \frac{2\pi N}{VkT}\int_d^\infty \phi(r)g(r/d)r^2\,dr - \ln(V/\Lambda^3) - 1, \quad (1)$$

where $g(r/d)$ is the hard-sphere distribution function, $\phi(r)$ is the pair potential, and $F^0(d, V)$ is the free energy of a system of hard spheres of diameter d and volume V. In general, d is a function of temperature: the higher the temperature, the smaller the effective size of the hard spheres. If for $g(r/d)$ we choose the Percus-Yevick[9] function, then Eq. (1) is considerably simplified since, as MC have shown, we can write this integral as

$$\int_d^\infty \phi(r)g(r/d)r^2\,dr = \int_0^\infty U(s)G(s)\,ds, \quad (2)$$

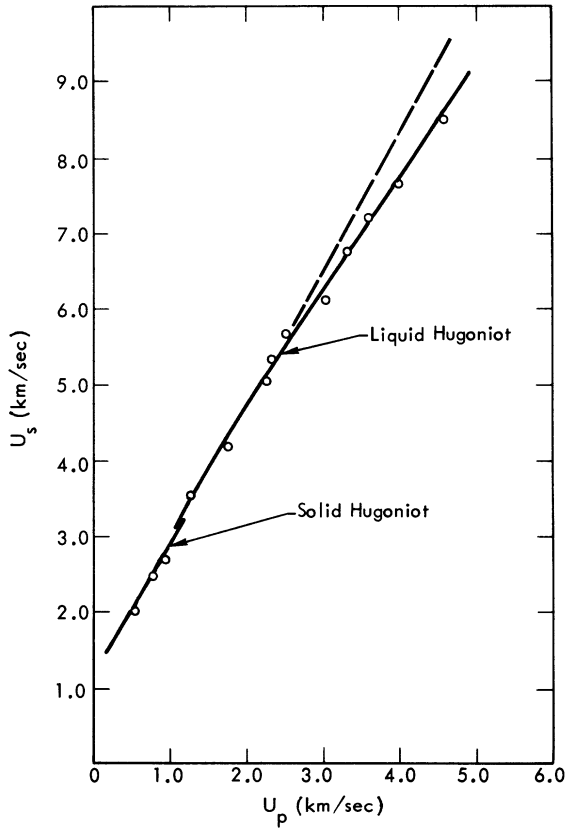

FIG. 1. Shock velocity (U_s) vs particle velocity (U_p) of solid argon shock compressed at 75 °K. The circles are results from Dick *et al.* The dashed line is an extension of the lower U_sU_p points to illustrate the curvature in the data. The solid lines are the calculated Hugoniots in the liquid and solid.

where $G(s)$ is the Laplace transform of $(r/d)g(r/d)$ and $U(s)$ is the inverse Laplace transform of $(r/d)\phi(r/d)$. $G(s)$ is known analytically. For a potential of the exponential-6 form,

$$\phi(r) = \epsilon\left[\left(\frac{6}{\alpha-6}\right)e^{\alpha(1-r/r^*)} - \left(\frac{a}{\alpha-6}\right)\left(\frac{r^*}{r}\right)^6\right], \quad (3)$$

we can now rewrite the integral in Eq. (1) as

$$\frac{2\pi N}{VkT}\int_0^\infty U(s)G(s)\,ds = \frac{12\eta}{T^*}e^\alpha\left(\frac{6}{\alpha-6}\right)[-G'(\alpha c = s)] - \frac{12d^3}{T^*}\left(\frac{\alpha}{\alpha-6}\right)\int_0^\infty \frac{G(s)s^4\,ds}{c^6 4!}. \quad (4)$$

$\eta = \frac{1}{6}\pi(N/V)d^3$, G' is the first derivative of G evaluated at $s = \alpha c$, $T^* = kT/\epsilon$, and $c = r^*/d$.

The first term on the right is the contribution to the integral of Eq. (2) from the exponential repulsive potential; it is done analytically. The second term is the integral arising from the attractive term. It is worth noting that for Morse potentials or screened Coulomb potentials, Eq. (2) can be expressed entirely analytically. Since $G(s)$ is known analytically in the Percus-Yevick theory, the second term is easily computed. As in Mansoori and Canfield, d is determined by minimizing the free energy, and thermodynamic properties are computed by taking the derivatives of the minimized free energy.

In our early work with this model we used the expression

$$F^0 = \frac{4\eta - 3\eta^2}{(1-\eta)^2}, \quad (5)$$

which accurately describes the free energy of the hard-sphere system as determined by molecular dynamics.

However, in computing the properties of systems interacting according to inverse 9th- and inverse 12th-power potentials, it was found that the function

$$F^0 = \frac{4\eta - 3\eta^2}{(1-\eta)^2} - \eta \quad (6)$$

was superior to Eq. (5) in that it would reproduce their properties as determined by Monte Carlo calculations to within 1%. Table I summarizes the comparison between Monte Carlo calculations, the LJD cell model, and the liquid models for the inverse 12th-power potential.[10] In Tables I and II $\rho = (r^{*3}/\sqrt{2})(N/V)$. Similar agreement is obtained in the case of the inverse 9th-power potential.

In Table II we have a calculation of PV/RT and the excess energy U/RT, using Eqs. (1) and (6) for a Lennard-Jones 12-6 potential versus Monte Carlo calculations at $kT/\epsilon = 2.74$. This temperature is twice the critical temperature in argon and is comparable with the lowest temperatures we will

TABLE I. Comparison between Monte Carlo calculations, the LJD cell model, and liquid models for the inverse-12th power potential.

	Solid (PV/RT)		Liquid (PV/RT)		
ρ	Monte Carlo [a]	LJD	Monte Carlo [a]	Eq. (6)	Eq. (5)
0.1			1.45	1.42	1.49
0.2			2.12	2.09	2.22
0.3			3.10	3.10	3.29
0.4			4.55	4.59	4.82
0.5			6.63	6.71	6.97
0.6			9.56	9.66	9.94
0.7			13.49	13.78	13.98
0.8	16.51	16.12	18.76	19.05	19.36
0.9	22.55	22.34			
1.0	30.99	30.85			
1.2	57.16	57.09			

[a] Reference 10.

be concerned with, the highest temperatures being of the order of 21 500 °K. In this temperature range we can compare the model to Monte Carlo calculations[11] for the exponential-6 potential of Eq. (3) with parameters $\alpha = 13.5$, $\epsilon/k = 122.0$ °K, and $r^* = 3.85$ Å, as shown in Tables III and IV. The agreement is quite good and covers a density range greater than that of the argon shock data. More recently, a number of workers[12] have developed perturbation theories of liquids to greater accuracy than MC. However, the newer formulations require considerably more labor, and for most applications such as the present one the additional accuracy is superfluous.

III. HUGONIOT CALCULATIONS

Figure 2 shows the experimental points of Dick *et al.* The solid curves are theoretical Hugoniot curves made with the models of the previous section and the exponential-6 potential of Eq. (3), where $\epsilon/k = 122.0$ °K, $r^* = 3.85$ Å, and $\alpha = 13.0$. These results are also shown in Table V with the computed temperatures. The upper solid curve in Fig. 2 is the Hugoniot computed with the liquid model, the lower solid curve was computed with the LJD model, and the dashed curve is the melting line determined in Sec. IV. The PV curve of a shocked material (Hugoniot) is determined by the relationship

$$E - E_0 = \tfrac{1}{2}(P + P_0)(V_0 - V), \tag{7}$$

where E, P, and V are the final energy, pressure, and volume and the subscripted terms are the initial conditions. The values of E_0, P_0, and V_0 are, respectively, -1523 cal/mol, 1 bar, and 24.21 cm^3/mol. To compute a Hugoniot curve, one chooses a temperature, computes E, P, and V along the isotherm, and then determines the pressure-volume point that satisfies Eq. (7).

The calculated U_sU_p curves of the liquid and solid model are also shown in Fig. 1. The lower solid line is the solid U_sU_p and the upper one is the liquid. Each has been discontinued near the predicted melting transition. Note the smallness of the break. It is clear that the nonlinearity is fully explained solely as a characteristic feature of the liquid-model Hugoniot and need not imply a phase transition.

In an earlier set of experiments on argon, van Thiel and Alder[1] shock compressed the liquid, initially at 86 °K and 1 bar, up to 365 kbars and a volume of 13.8 cm^3/mol. In analyzing that set of data, we found that the best fit to the data was obtained using an exponential-6 potential with $\alpha = 13.5$, $\epsilon/k = 122.0$ °K, and $r^* = 3.85$ Å; but because of the large error bar, $\alpha = 13.0$ or $\alpha = 14.0$ could be considered consistent with their data. We may then conclude that the results of van Thiel and Alder, and Dick *et al.* are consistent within the order of their error bars, but they are not in excellent agreement.

The set of parameters chosen here are in no way unique. Dick *et al.*, in analyzing their data, computed the entire Hugoniot (including the liquid) using the solidlike LJD model and an exponential-6 potential with somewhat different parameters. In reality, the functional form chosen here is oversimplified. Barker and his co-workers[13] have shown that the complete potential for argon is more

TABLE II. Model calculations vs Monte Carlo at $kT/\epsilon = 2.74$ for Lennard-Jones potential.

	Monte Carlo [a]		Perturbation theory	
ρ	PV/RT	U/RT	PV/RT	U/RT
0.1	0.97	−0.22	0.95	−0.20
0.2	0.99	−0.44	0.94	−0.41
0.3	1.04	−0.65	0.98	−0.63
0.4	1.20	−0.87	1.12	−0.86
0.7	2.64	−1.42	2.62	−1.45
0.8	3.60	−1.56	3.74	−1.56
0.9	5.14	−1.61	5.33	−1.60
1.0	7.39	−1.53	7.54	−1.53

[a] Reference 12(a).

TABLE III. Model calculations vs Monte Carlo at $kT/\epsilon = 20$ for Eq. (3); $\alpha = 13.5$, $r^* = 3.85$Å, $\epsilon/k = 122$°K.

	Monte Carlo [a]		Perturbation theory	
ρ	PV/RT	U/RT	PV/RT	U/RT
0.9	3.27	0.28	3.32	0.26
1.0	3.81	0.38	3.89	0.37
1.25	5.52	0.73	5.73	0.76
1.50	8.07	1.34	8.28	1.36
1.75	11.34	2.17	11.65	2.22

[a] Reference 11.

TABLE IV. Model calculations vs Monte Carlo at $kT/\epsilon = 100$ for Eq. (3); $\alpha = 13.5$, $r^* = 3.85$Å, $\epsilon/k = 122$°K.

ρ	Monte Carlo [a] PV/RT	Monte Carlo [a] U/RT	Perturbation theory PV/RT	Perturbation theory U/RT
1.264	3.06	0.55	3.13	0.55
1.473	3.71	0.74	3.81	0.75
1.768	4.80	1.08	4.94	1.10
2.431	8.17	2.20	8.41	2.25
2.701	9.86	2.78	10.22	2.88

[a] Reference 11.

TABLE V. Calculated Hugoniots.

V(cm^3/mol)	LJD P(kbar)	LJD T(°K)	Perturbation theory P(kbar)	Perturbation theory T(°K)
20.00	8.03	147.1	9.45	113.5
17.41	24.86	332.4	29.00	282.8
16.44	38.34	525.1	45.19	474.6
15.71	53.80	779.2	63.89	741.6
15.35	63.93	960.6	76.08	937.6
13.90	134.4	2435	157.7	2576
13.22	196.7	3939	225.3	4235
12.30	343.0	7892	371.2	8423
11.57	555.8	14185	561.4	14710
11.09			744.5	21376

complicated and has a well depth about 20 °K deeper. However, because of their simplicity, functional forms will continue to be useful. As a result of the high temperatures and densities achieved in shock experiments, the largest contributions to the thermodynamic properties arise from small interatomic separations on the repulsive side of the potential function. For example, at 12 000 °K the maximum contribution to the total pressure arises from interactions of pairs of atoms at an average separation of 2.3 Å. (The potential minimum is at 3.85 Å.) Therefore, our pair potential should accurately represent the repulsive pair potential, and we will not be concerned as to whether the potential reproduces the entire argon equation of state. This can only be done by the more complete methods used by Barker.

That our potential is accurate in the repulsive region can be seen in Fig. 3, which shows the exponential-6 potential of Eq. (3) plotted against the M.I.T.[14] molecular beam results. The maximum disagreement is about 20%. The over-all agreement is good and within the combined experimental error.

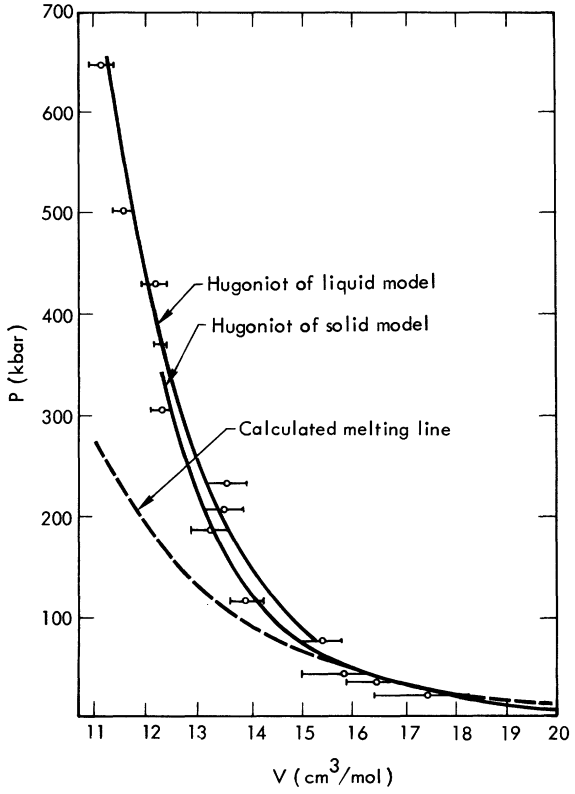

FIG. 2. Hugoniot curve of argon. The bars are experimental points from Dick *et al.*

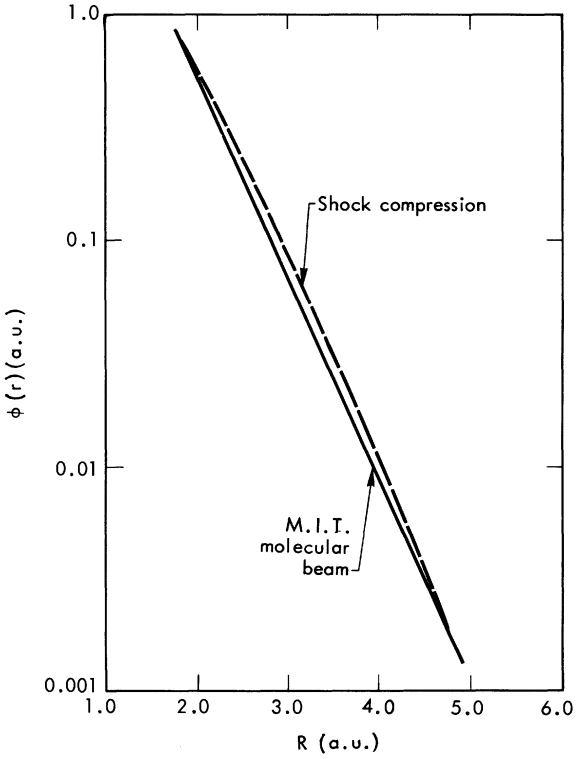

FIG. 3. Comparison of intermolecular potentials obtained from molecular-beam scattering and from the present analysis of the shock-compression work.

Recently Seitz and Wackerle[15] have reported measurements in which liquid argon initially at 86 °K and 1 bar was shock compressed to 14.0 cm^3/mol and 257 kbars, and then this first shock wave was reflected off a metal alloy plate to achieve still higher pressures up to 740 kbars and a volume of 9.87 cm^3/mol. Their results are shown in Fig. 4. Also shown are our calculations using the fluid model and the potential with $\alpha = 13.0$. The calculation of the primary Hugoniot was started from the liquid at a temperature of 86 °K and a volume of 28.4 cm^3/mol and is represented by a dashed line. Note that a portion of the volume scale has been omitted. The reflected Hugoniot was computed by using the E, P, and V of the primary Hugoniot at 14.0 cm^3/mol as the E_0, P_0, and V_0 of the reflected Hugoniot and solving Eq. (7) at smaller volumes. The agreement between theory and experiment is quite good at the lower pressures, but it deteriorates progressively at higher pressures. On taking into account the difficult nature of reflected-shock experiments, we consider the over-all agreement to be satisfactory.

These experiments by Seitz and Wackerle have clarified a point that had been troublesome in the past. In 1966 in a pioneering experiment van Thiel and Alder[1] reported the reflected points shown in Fig. 4 as the dashed bars. In analyzing the data, we found these reflected points totally inconsistent with the primary Hugoniot, unless we assumed the possibility of metallization. However, electron-band calculations on argon predicted that metallization would not occur until 4.5 cm^3/mol.[4,16] Since the experiments of Seitz and Wackerle are consistent with all the other shock-wave work on argon, including the primary Hugoniot of van Thiel and Alder, we must conclude that the early reflected experiments of van Thiel were in error. The Seitz-Wackerle results also allow us to conclude that metallization in argon has not occurred down to 9.9 cm^3/mol.

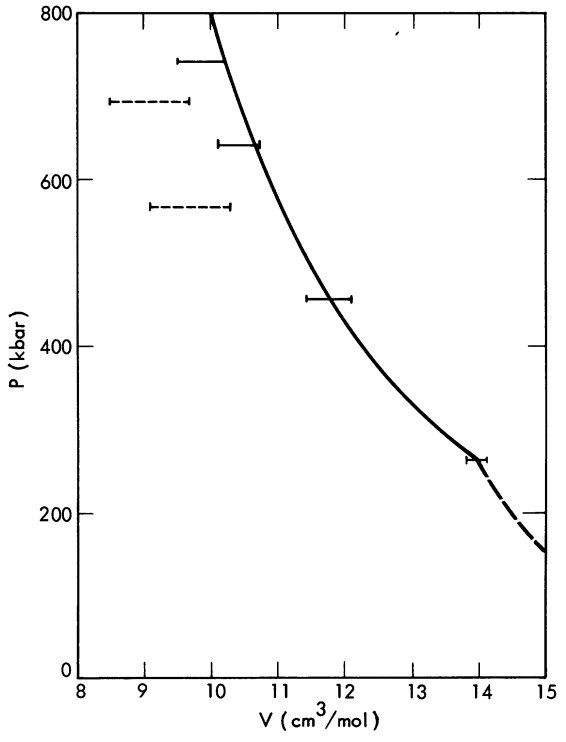

FIG. 4. Reflected argon Hugoniot. The solid bars are data from Seitz and Wackerle. The dashed bars are data of van Thiel and Alder. The dashed curve is the calculated primary Hugoniot, and the solid curve is the reflected Hugoniot.

IV. THEORETICAL MELTING CURVES

As is well known, the thermodynamic conditions for melting require thermal, mechanical, and chemical equilibrium. These can be summarized as

$$T_s = T_f, \quad P_s = P_f, \quad G_s(P, T) = G_f(P, T). \tag{8}$$

The quantities temperature, pressure, and Gibbs free energy must be the same in the solid and fluid phases. In a rigorous first-principles calculation of a melting curve it is necessary to have determined an intermolecular potential and then to calculate the equation of state by some statistical model. In computer experiments one can assume an intermolecular function such as the Lennard-Jones potential or inverse-power potentials, then calculate the thermodynamic properties exactly over a wide range of solid and liquid densities, and determine the melting curve. However, these experiments require a large amount of computer time and are not practical for studying a wide range of potentials. Therefore, it is desirable to use approximate models. The great value of computer experiments is that they provide us with precise measurements for an assumed pair potential and thereby allow us to compare approximate models to exact results.

Approximate models fall into two categories. In one, an attempt is made to compute the pressure and free energy for the two phases and determine the melting curve using the equilibrium conditions. The difficulty with this approach is that while the pressure may be calculated accurately, relatively small errors in the free energy may, as will be seen below, lead to highly erroneous results. It is for this reason that a second approach, involving the properties of only a single phase, has been widely used. The Lindemann and Simon melting laws are well-known examples in the latter category.

The models used in this section have been discussed at some length in a recent review article,[17] where their use was justified by comparing their predictions with the results of computer experiments. In order to avoid repetitious discussions, we refer the reader to that article. First we calculate the high-pressure melting curve of argon by using the statistical models of Sec. II to compute the thermodynamic properties of each phase, and we use the intermolecular potential obtained from the shock data. To test our calculations we compare our result to the high-pressure melting points determined by Stishov *et al.*[18] at 322 °K and 15.8 kbars and by Crawford and Daniels[19] at 201.32 °K and 6.34 kbars. We determined the melting points by using the LJD model and the MC perturbation theory to calculate the free energy and pressure of the solid and liquid. Calculations were made using Eqs. (5) and (6) for the hard-sphere free energy. The results are shown in Table VI. We find that the model giving the better description of the equation of state [Eq. (6)] gives poorer agreement with the experimental melting point. To understand this, we look at the Helmholtz free energies of these approximate models for the case of the inverse 12th-power potential versus the exact computer calculations as shown in Fig. 5. In practice, it is easiest to determine the liquid-solid phase transition by finding the volume at which the metastable extensions of two phases have the same Helmholtz free energy and then using the equal-area rule to find the pressure corresponding to equal Gibbs free energy. In Fig. 5 we see that the LJD model and the perturbation theory with Eq. (5) are *both* incorrect by approximately 0.45 units (5%) at the transition, and as a result they make predictions that are in excellent agreement with the computer results. The PV/NKT for the LJD cell model, both perturbation models, and the Monte Carlo calculations for the inverse-12th-power potential were given in Table I. The overall agreement of the approximate models with Monte Carlo results was seen to be very good, and the two models of the liquid differ in pressure by a relatively small amount. However, the difference in their free energies is equal to the integral of this pressure difference from $\rho = 0$ and is large enough to throw the predicted transition badly off. While a 5% model of the pressure is usually adequate for practical purposes, such an error in the free energy of one of the phases (see Fig. 4) may be disastrous. An accurate free energy is then more important to melting calculations than an accurate pressure. Thus, in improving our equations of state by using Eq. (6) for F^0, we have destroyed a fortuitous cancellation. We therefore make use of this cancellation by using the LJD model and the perturbation theory with Eq. (5) to compute the melting curve to 1200 °K. The results are shown in Table V and are plotted as closed circles in Fig. 6.

Because, as we have shown, melting transitions are sensitive to small free-energy differences, it is in practice worthwhile to consider simpler one-phase models that are less fundamental but just as accurate. The one-phase melting models used here are based on the LJD cell model and the hard-

TABLE VI. Calculated melting points vs experiment.

T (°K)	P (kbar)	V_s (cm^3/mol)	V_L (cm^3/mol)
201.3 [a]	6.34	21.69	23.10
201.3 [b]	6.45	21.80	22.97
201.3 [c]	12.80	18.90	20.10
322 [d]	15.84	19.40	20.40
322 [b]	15.70	19.10	20.40
322 [c]	28.80	16.85	17.60

[a] Experimental results of Crawford and Daniels (Ref. 19).
[b] Computed using LJD model and MC theory with Eq. (5).
[c] Computed using LJD model and MC theory with Eq. (6).
[d] Experimental results of Stishov (Ref.18).

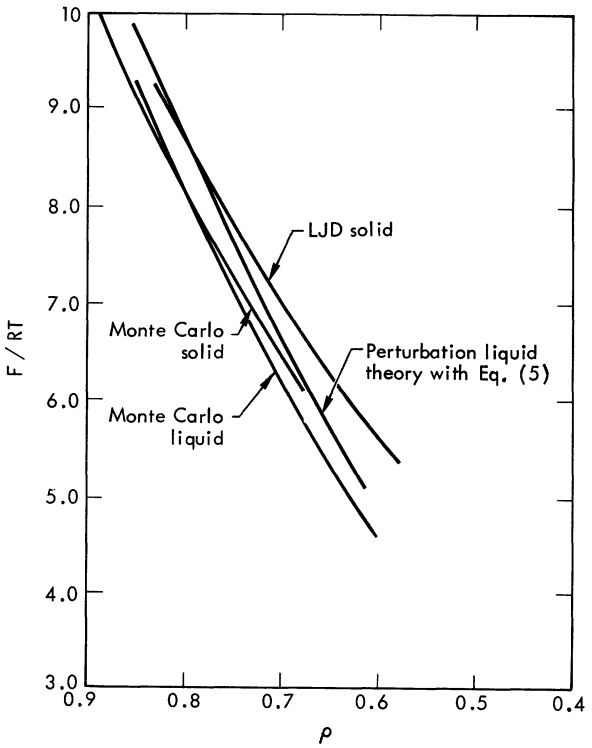

FIG. 5. Excess free energy of a system of particles interacting according to the inverse 12th-power potential (Ref. 10).

sphere fluid. One point of view, which is originally due to Lindemann, is that at each density along the melting curve the average arrangement of the atoms in some suitably reduced dimension is always the same. A similar statement can be made for the fluid. In the LJD cell model the partition function Z for a system of N localized atoms, each occupying a volume V, is written as

$$Z_{\text{cell}} = e^{\phi_0/kT}(V/N\Lambda^3)^N v_f^{*N}$$

and

$$v_f^* = (N/V)\int_\Delta e^{-\delta\phi/kT} d^3r, \tag{9}$$

where ϕ_0 is the potential energy of the stationary lattice and $\delta\phi$ is the change in potential energy of the system when the single particle wanders from its lattice site to r.

A model for melting based on the LJD model assumes that the scaled one-particle partition function v_f^* is a constant along the melting curve. This model is a generalization of the Lindemann law, which states that the ratio of the root-mean-squared displacement to the nearest-neighbor spacing is a constant along the melting curve. The generalization is carried out by assuming that the ratio of the one-particle partition function [the integral in Eq. (9)] to the atomic volume is a constant along the melting curve. This ratio is defined in Eq. (9) as v_f^*.

In applying this model we find v_f^* on the experimental curve at 322 °K and 19.4 cm^3/mol ($v_f^* = 4.24 \times 10^{-3}$) and determine the pressures and volumes that have this value of v_f^* at higher temperatures, thus determining the melting curve. These results, which are shown as the lower dashed curve on Fig. 6 and in parenthesis in the third column of Table VII, are in excellent agreement with our previous calculations based on thermodynamic considerations.

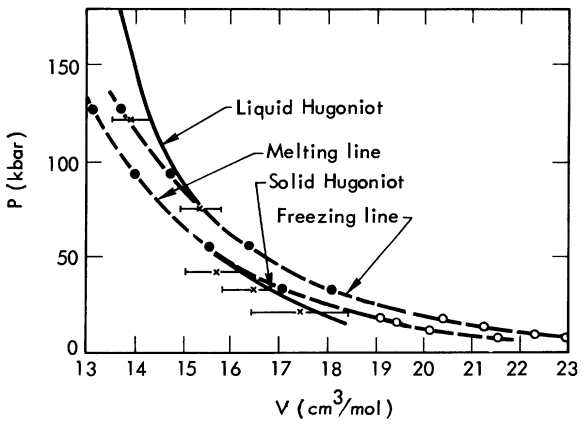

FIG. 6. The Hugoniot curve of solid argon near the melting transition. The bars are experimental points from Dick *et al.* The open circles are melting and freezing points from Stishov. The closed circles are results of the computations in Table VII.

The liquid analog of the Lindemann law assumes that all along the freezing curve the ratio of the "effective" hard-sphere volume of the atoms to the total volume is a constant. In other words, the η defined in Sec. II is a constant along the freezing line. Using perturbation theory [with Eq. (6)], we determined the value of η at $T = 322$ °K and $V = 20.4$ cm^3/mol and computed the freezing curve shown in Fig. 6 and in parenthesis in the fourth column of Table VII. η is equal to 0.4537. There is also excellent agreement with our previous calculations.

These results show that the Hugoniot should pass out of the solid at about 55 kbars and into the liquid at 70 kbars, and that unfortunately the experimental error is larger than the volume change on melting at constant temperature. As a result, it is not possible to determine from the data if the melting curve is where we have predicted it to be. It may be that the large experimental error of the low-pressure points is due to the proximity of the melting curve. It is also clear that, because of the small angle at which the Hugoniot intersects the melting curve, any experiment will need to be accurate to about ± 0.1 cm^3/mol to produce useful information. The experimental error bars in the solid range from ± 0.63 to ± 0.99 cm^3/mol. Even the U_sU_p curve in Fig. 1, which might be a more sensitive indicator of a transition than PV, shows only a small break in the two curves that is much less than the experimental error.

The question then arises: Is there a diagnostic technique other than U_sU_p or PV by which a phase transition might be detected? An affirmative answer to this is given by Sakharov and co-workers,[20,21] who were able to measure viscosity of substances behind a shock front using a method based on the creation of small disturbances of known wavelength in the front. These authors studied aluminum, lead, and sodium chloride and were able to interpret a sudden drop in viscosity as being due to melting. However, not enough

TABLE VII. Calculated melting points.

T (°K)	P (kbar)	V_s (cm^3/mol)	V_L (cm^3/mol)
201.3	6.45	21.80	22.97
322	15.70	19.10	20.40
500	32.0	17.05 (17.22)	18.05 (18.04)
700	54.5	15.55 (15.61)	16.35 (16.28)
1000	92.5	14.00 (13.96)	14.70 (14.54)
1200	127.8	13.15 (13.17)	13.85 (13.63)

points were taken to accurately determine the melting points. Inasmuch as most materials have Hugoniots and melting curves similarly interrelated, as in argon, it would seem that viscosity, or some measurement that depended upon the structure of the substance rather than the thermodynamic properties is necessary to determine the melting curve.

V. APPROXIMATE CALCULATION OF REPULSIVE POTENTIAL

Intermolecular forces are, in principle, computable by *ab initio* methods for small atoms such as helium, but they are as yet not generally practical. At present the most reliable way to get these forces is by the analysis of experimental data or via molecular-beam experiments. However, often the relevant data are unavailable and a simple calculation would be useful even if it were not highly accurate. In this section we discuss a simple method for computing just the repulsive part of the potential and compare it to the repulsive part of our potential from shock-compression data.

Hafmeister[22] pursued a method suggested by Dick and Overhauser[23] and calculated the repulsive intermolecular potentials for a number of systems using the equation

$$\phi(R_{ij}) = \frac{2}{R_{ij}}\left[\sum_{n,m}\int u_i^n(\vec{r})u_j^m(\vec{r})\,d\vec{r}\right]^2, \qquad (10)$$

where u_i^n and u_j^m are the nth and mth atomic orbitals centered on atoms i and j whose centers are separated by a distance R_{ij}, and $\phi(R_{ij})$ is their energy of interaction. The justification for this approximation has been discussed at some length by these authors. It is important to note that the integral is an overlap integral and the repulsion is proportional to the overlap of the wave functions. Hafmeister evaluated these integrals by direct numerical integration using Hartree-Fock wave functions and calculated $\phi(R_{ij})$ near the normal density of the solid ($R = 7.2$ a.u.). His results were in agreement with empirical potentials obtained from low-pressure gas and solid data. Since the temperatures attained in shock-wave experiments are up to about 21 000 °K (an energy of 0.08 a.u.), we expect contributions to the shock curves to come from all internuclear separations down to about 4.2 a.u. as seen from the plot of $\phi(R)$ vs R in Fig. 7. Our intention is to use a simplified form of Hafmeister's method to calculate the repulsive intermolecular potential at the much smaller interatomic spacings found in shock-wave experiments. Equation (10) was originally obtained by a perturbation approach, and it is only valid for small overlaps of the wave functions on atoms i and j. In this region the tails of the wave functions can be fitted quite accurately to exponential functions, and the overlap integrals can be evaluated analytically. We have followed this simplified procedure for argon by fitting the $3s$ and $3p$ Hartree-Fock and Hartree-Fock-Slater wave functions outside the outermost maximum to an exponential function of the form

$$u(r) = Ae^{-Br}P_m^l, \qquad (11)$$

where P_m^l is the appropriate Legendre polynomial. A and B are determined by the fitting to the wave function. The integrals in Eq. (10) can then be performed analytically[24] by using Eq. (11).

The Hartree-Fock wave functions were taken from the work of Mann.[25] The Hartree-Fock-Slater functions were calculated from the Herman-Skillman program.[26] In the Hartree-Fock-Slater method, the exact exchange term in the one-electron Hamiltonian is replaced by an average local exchange of the form $-f3[(3/\pi)\rho(r)]^{1/3}$. When $f = 1$,

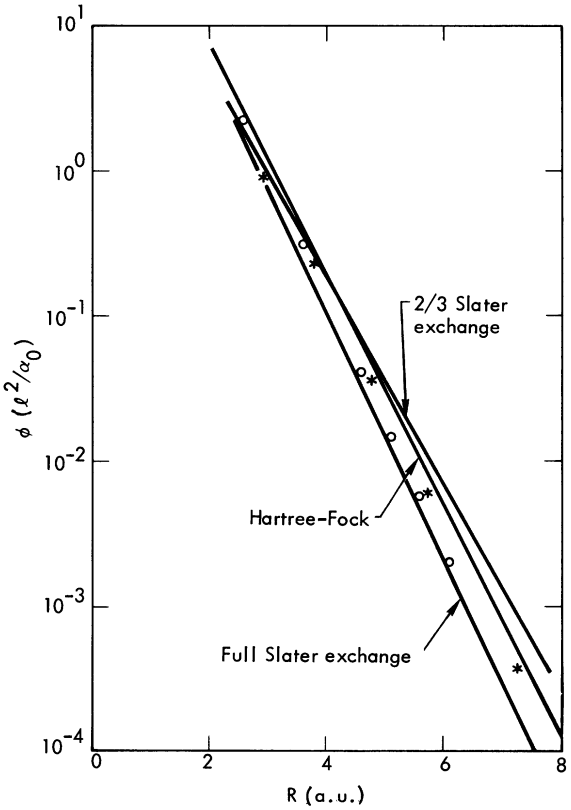

FIG. 7. Calculation of the repulsive potential. The solid curves were calculated using the indicated exchange approximation. The repulsive potential obtained from the analysis of shock data [i.e., the repulsive part of Eq. (3)] is indicated by stars. The repulsive potential calculated by Abrahamson from the TFD model is represented by open circles.

we have what is known as the Slater exchange, and when it is $\frac{2}{3}$, we have the Kohn-Sham-Gasper exchange. These averaged exchange potentials are used to solve self-consistently the one-electron Schröndinger equation,

$$\epsilon_i u_i = \{-\nabla^2 + V(r) - f3[(3/\pi)\rho(r)]^{1/3}\} u_i ,$$

where $V(r)$ is the Coulomb potential. The computed u_i were fitted to Eq. (11) and $\phi(R_{ij})$ was calculated. Figure 6 shows the results of these calculations and compares them with the repulsive part of the intermolecular potential obtained from shock data. Also shown are the results of Abrahamson[27] from TFD theory. The agreement with experiment is best for the calculations made with the Hartree-Fock functions. Hafmeister's exact calculations at 7.2 a.u. were also made using Mann's Hartree-Fock functions, and our approximate results are within 2% of his. At smaller internuclear separations the overlaps will increase, and both Eq. (10) and Eq. (11) will become increasingly less adequate, which may be the reason for the crossing of the Hartree-Fock and $f = \frac{2}{3}$ exchange curves. Nevertheless, these calculations require only a minimal effort, they are accurate to within the experimental determination, and they appear to present a very simple but satisfactory method of estimating repulsive intermolecular forces between closed-shell atoms.

In recent years a considerable controversy has arisen over the merits of the $f = 1$ and $f = \frac{2}{3}$ exchange factors, concerning which is superior as a replacement for the exact Hartree-Fock exchange potential. It has become apparent that the best replacement is given by some intermediate value. For argon, Kmetko[28] estimates this value to be 0.75. He bases his estimate on calculations that show that wave functions calculated with this value of f, when placed in the Hartree-Fock equations for the total energy, give the lowest energy of all the values of f. The results in Fig. 7 are qualitatively consistent with these calculations. The experimental results are in best agreement with the Hartree-Fock results, and they lie between the two approximate exchange factors.

---

*Work performed under the auspices of the U. S. Atomic Energy Commission.

[1]M. van Thiel and B. J. Alder, J. Chem. Phys. **44**, 1056 (1966).
[2]M. Ross and B. J. Alder, J. Chem. Phys. **46**, 4203 (1967).
[3]M. Ross and B. J. Alder, J. Chem. Phys. **47**, 4129 (1967).
[4]M. Ross, Phys. Rev. **171**, 777 (1968).
[5]R. D. Dick, R. H. Warnes, and J. Skalyo, Jr., J. Chem. Phys. **53**, 1648 (1970).
[6]J. E. Lennard-Jones and A. F. Devonshire, Proc. R. Soc. Lond. **A163**, 53 (1957).
[7]G. A. Mansoori and F. B. Canfield, J. Chem. Phys. **51**, 4958 (1969).
[8]J. A. Barker, *Lattice Theories of the Liquid State* (Macmillan, New York, 1963).
[9]M. S. Wertheim, Phys. Rev. Lett. **10**, 321 (1963).
[10]W. G. Hoover, M. Ross, K. W. Johnson, D. Henderson, J. A. Barker, and B. C. Brown, J. Chem. Phys. **52**, 4931 (1970).
[11]M. Ross and B. J. Alder, J. Chem. Phys. **46**, 4203 (1967).
[12](a) L. Verlet and J. J. Weis, Phys. Rev. A **5**, 939 (1972); (b) J. D. Weeks, D. Chandler, and H. C. Anderson, J. Chem. Phys. **54**, 5237 (1971).
[13]J. A. Barker, M. V. Bobetic, and A. Pompe, Mol. Phys. **20**, 347 (1971); J. A. Barker, R. A. Fisher, and R. O. Watts, Mol. Phys. **21**, 657 (1971); J. A. Barker and M. L. Klein, Chem. Phys. Lett. **11**, 501 (1971).
[14]S. O. Colgate, J. E. Jordan, I. Amdur, and E. A. Mason, J. Chem. Phys. **51**, 968 (1969).
[15]W. L. Seitz and J. Wackerle, Bull. Am. Phys. Soc. **17**, 1093 (1972).
[16]D. Brust, M. Ross, and K. Johnson, J. Nonmetals 1, 47 (1972).
[17]W. G. Hoover and M. Ross, Contemp. Phys. **12**, 339 (1971).
[18]S. M. Stishov, I. N. Makerenko, V. A. Ivanov, and V. I. Fedosimov, Zh. Eksp. Teor. Fiz. Pis'ma Red. **11**, 22 (1970) [JETP Lett. 11, 13 (1970)].
[19]R. K. Crawford and W. B. Daniels, Phys. Rev. Lett. **21**, 367 (1968).
[20]A. D. Sakharov, R. M. Zaidel, V. N. Mineev, and A. G. Oleinik, Dokl. Akad. Nauk SSSR **159**, 1019 (1964) [Sov. Phys.-Dokl. **9**, 1091 (1965)].
[21]V. N. Mineev and E. V. Savinov, Zh. Eksp. Teor. Fiz. **52**, 629 (1967) [Sov. Phys.-JETP **25**, 411 (1967)].
[22]D. W. Hafmeister and W. H. Flygore, J. Chem. Phys. **43**, 795 (1965); D. W. Hafmeister, J. Phys. Chem. Solids **30**, 117 (1969).
[23]B. G. Dick and A. W. Overhauser, Phys. Rev. **112**, 90 (1958).
[24]C. A. Coulson, Proc. Camb. Philos. Soc. **38**, 210 (1942).
[25]J. B. Mann, Los Alamos Scientific Laboratory, Report No. LA-3690, 1967 (unpublished).
[26]F. Herman and S. Skillman, *Atomic Structure Calculations* (Prentice-Hall, Englewood Cliffs, N. J., 1963).
[27]A. A. Abrahamson, Phys. Rev. **130**, 693 (1963).
[28]E. A. Kmetko, Phys. Rev. A **1**, 37 (1970).